# **Article**



# Controlling heme redox properties in peptide amphiphile fibers with sequence and heme loading ratio

Chiranjit Dutta, <sup>1</sup> Virginia Lopez, <sup>1</sup> Conner Preston, <sup>1</sup> Nimesh Rudra, <sup>2</sup> Alex Mauricio Valdivia Chavez, <sup>1</sup> Abigail M. Rogers, <sup>3</sup> and Lee A. Solomon<sup>1,\*</sup>

<sup>1</sup>Department of Chemistry and Biochemistry, George Mason University, Fairfax, Virginia; <sup>2</sup>Thomas Jefferson High School for Science and Technology, Alexandria, Virginia; and <sup>3</sup>Department of Biology, George Mason University, Fairfax, Virginia

ABSTRACT Controlling the reduction midpoint potential of heme B is a key factor in many bioelectrochemical reactions, including long-range electron transport. Currently, there are a number of globular model protein systems to study this biophysical parameter; however, there are none for large polymeric protein model systems (e.g., the OmcS protein from *G. sulfurreducens*). Peptide amphiphiles, short peptides with a lipid tail that polymerize into fibrous structures, fill this gap. Here, we show a peptide amphiphile model system where one can tune the electrochemical potential of heme B by changing the loading ratio and peptide sequence. Changing the loading ratio resulted in the most significant increase, with values as high as  $-22 \, \text{mV}$  down to  $-224 \, \text{mV}$ . Circular dichroism spectra of certain sequences show Cotton effects at lower loading ratios that disappear as more heme B is added, indicating an ordered environment that becomes disrupted if heme B is overpacked. These findings can contribute to the design of functional self-assembling biomaterials.

SIGNIFICANCE Many polymeric proteins can transport electrons; however, no model systems exist to study them. We provide, to the best of our knowledge, the first peptide-polymeric model system that can bind heme B and carry out tuneable oxidation/reduction activity. In this article, we perform initial characterizations on this system to show how the redox properties can be tuned to match natural proteins and what is likely happening in the system. We believe many researchers who study polymeric electron transport proteins will want to use this model system to study the underlying biophysics of their complex natural systems.

# INTRODUCTION

Metalloproteins are widely studied due to their active role in biological systems. Proteins utilize metal ions, metal-containing cofactors, or prosthetic groups to catalyze crucial functions including respiration and water oxidation (1,2). Heme is an iron-containing porphyrin that serves as the prosthetic moiety of hemoproteins, which carry out vital and diverse functions including oxygen binding and waste processing. Understanding these functions has been the topic of a number of studies over many years, in both natural and de novo systems, from which we have developed a thorough understanding of how heme reduction properties are

controlled (1–16). However, no model systems of polymeric peptides or biomaterials exist to study heme properties, and therefore it is unclear whether many of the principles carry over or what parameters change. This paper shows the development and characterization of a polymeric peptide model system to fill this gap.

Polymeric metalloprotein fibers undergo a number of electron transport functions (17). The OmcS protein (18) from *G. sulfurreducens* and the MtrCAB protein (19) from *S. oneidensis* are two well-known examples. These two proteins use 6- and 20-heme subunits, respectively, to transport electrons over micron distances. In both cases, it is observed that the heme cofactors are kept in a precise arrangement to one another, often as stacked pairs. Recent work by Jiang et al. sought to compare the two proteins through MD simulations and decipher what about their structures leads to differences in their electron transport rates and abilities (20). However, due to the proteins' inherent complexities,

Submitted April 3, 2024, and accepted for publication May 21, 2024.

\*Correspondence: lsolomo@gmu.edu

Chiranjit Dutta and Virginia Lopez authors contributed equally to this work.

Editor: Ronald Koder.

https://doi.org/10.1016/j.bpj.2024.05.021

© 2024 Biophysical Society.



these results can be skewed. Dahl et al. recently noted that there is even debate and a lack of clear evidence to explain the specific mechanism of electron transport and the conductivity that is observed in both of these proteins (21). A new model system is therefore required to probe the fundamental biophysical elements, which can then be applied back to these natural proteins and help explain their function.

Simplified model systems remove much of the protein complexity and allow for a more direct probing of protein function (12,22-29). The ideal model system must have a simple sequence, which allows for minor changes to have a larger impact on function. There have been studies that remove the protein entirely (30,31); however, the role of protein has been shown to be important, and therefore function cannot be fully explained without it. Simulation-based studies have also been done on these systems (32,33); however, it is unclear whether those results are being biased by unforeseen complexities in the protein architecture. Peptide amphiphiles (PAs) are excellent candidates to function as a model system for polymeric proteins. They reproduce the amino acid environment of natural proteins, but in a simplified way, where small changes have a large effect. Similarly, they provide an easier computational system with fewer atoms to model function.

PAs are a class of polymeric peptides defined by their short peptide headgroup attached to a lipid tail (34,35). Importantly, they offer a simplified system in which fundamental biophysical principles of electron transport can be studied as they lack the complexity that plagues natural proteins. The PAs we use have the added advantage of binding the redox active cofactor, heme B (36). Past work has sought to investigate how these materials can control the bioelectrochemical properties of heme B (36,37). Solomon et al. modulated the functional region of the peptide to characterize peroxidase function (36).

Here, we use PAs as a model system to probe the effects of polymeric protein structure and heme stacking on the reduction potential. We created a series of peptides with different structural regions and porphyrin loading ratios and carried out redox titrations to measure their effect on the midpoint potential. We demonstrate a significant shift upward in heme B reduction potential as a function of the burial away from water, the proximity to positive surface charges, and the ratio of heme B in the materials themselves. Our work demonstrates that these peptide materials can be a useful model system to study functions such as long-range electron transport, or oxygen binding, in protein polymers (38) and to investigate the role of heme B cofactor organization on a few biophysical properties. These findings can then be used in the design of functional electron transport model systems or for the development of functional biomaterials that utilize the heme B cofactor over a wide reduction potential range.

### MATERIALS AND METHODS

### Materials

All reagents for peptide synthesis were procured from Sigma-Aldrich (St. Louis, MO, USA) unless stated otherwise. Milli-Q water was used to prepare all buffers in biophysical experiments, such as circular dichroism (CD).

### Methods

# Peptide synthesis

PAs were synthesized using conventional solid-phase chemistry in an automated peptide synthesizer. The synthesis employed Rink amide AM resin, which was swelled in dichloromethane and dimethylformamide (DMF) for 2 h. Fmoc deprotection was performed with 3 mL of 20% piperidine in DMF. After deprotection, the resin was filtered and washed with DMF (2×, 3 mL). Coupling was carried out using O-(1H-6-Chlorobenzotriazole-1-yl)-1,1,3,3-tetramethyluronium hexafluorophosphate (HCTU) (3 equiv) and Oxyma (3 equiv) in DMF for 20 min at 75°C. This process was repeated twice. The resin was filtered and washed with DMF (2 mL).

Prior to cleavage, the resin was transferred to a sintered glass vessel and washed with DMF (4×, 3 mL) and dichloromethane (5×, 2 mL). The cleavage step was performed under acidic conditions using trifluoro acetic acid (TFA) (95%)/triisopropylsilane (TIS) (2.5%)/H<sub>2</sub>O (2.5%) for 4 h. The resulting filtrates were evaporated. Purity was assessed by analytical highperformance liquid chromatography (C18 column, method: 10%-100%B/ 10 min, A: Milli-Q H2O + 0.1% TFA, B: acetonitrile (ACN) + 0.1% TFA, flow = 1 mL/min,  $T = 50^{\circ}$ C,  $\lambda = 214$  nm). The product was purified by preparative high-performance liquid chromatography (Phenomenex C18ec column, method: 40%-100%B/20 min, A: Milli-Q H2O + 0.1% TFA, B: ACN + 0.1% TFA, flow = 5 mL/min,  $\lambda =$  214 nm) and lyophilized to obtain a powder. Peptide mass was confirmed by MALDI-TOF.

### Circular dichroism

The secondary structure of peptides was determined using circular dichroism (CD) in a J-1100 CD spectrophotometer (Jasco) with a quartz cuvette having a path length of 1 mm. To confirm the secondary structure, the spectra of peptides were recorded at both pH 7 and 11 using concentrations of 300 and 100  $\mu$ M, respectively. Samples were prepared in 10 mM HEPES and 5 mM NH<sub>4</sub>OH for the corresponding pH and allowed to incubate at 90°C for 10 min. Data were collected at 20°C within the wavelength range of 190-240 nm at 0.2 nm intervals, with a scanning speed of 50 nm/min and three accumulations. The data were plotted using OriginPro 8.5 after subtracting the blank.

To understand the stacking of heme B within the peptide-heme complex, spectra of peptide-heme complexes were compared to the spectra of peptide-zinc protoporphyrin IX (ZnPPIX) complexes. Samples were prepared in 5 mM NH<sub>4</sub>OH at 300 or 500  $\mu$ M with 50  $\mu$ M heme B or ZnPPIX for loading ratios of 1:6 and 1:10, respectively. Samples were incubated at 90°C for 10 min and allowed to cool to room temperature before measurement. Data were collected at 20°C within the wavelength range of 350-500 nm at 0.2 nm intervals, with a scanning speed of 50 nm/min and three accumulations. The data were plotted using OriginPro 8.5 after subtracting the blank.

# Atomic force microscopy imaging

The self-assembly of peptides and peptide-heme complexes was imaged using atomic force microscopy (AFM) at both pH 7 and 11. The peptide and peptide-heme samples were prepared by dissolving them in 5 mM NH<sub>4</sub>OH and incubating them at 90°C for 10 min at pH 11 or dissolving them in 10 mM HEPES buffer at pH 7. A few microliters (5  $\mu$ L) of the sample were drop cast onto mica and allowed to dry at room temperature. The final concentration of peptide samples was 10  $\mu$ M. Imaging was performed using Nanosurf AFM with a contact mode cantilever tip (force constant: 0.2 N/m; resonance frequency: 13 kHz).

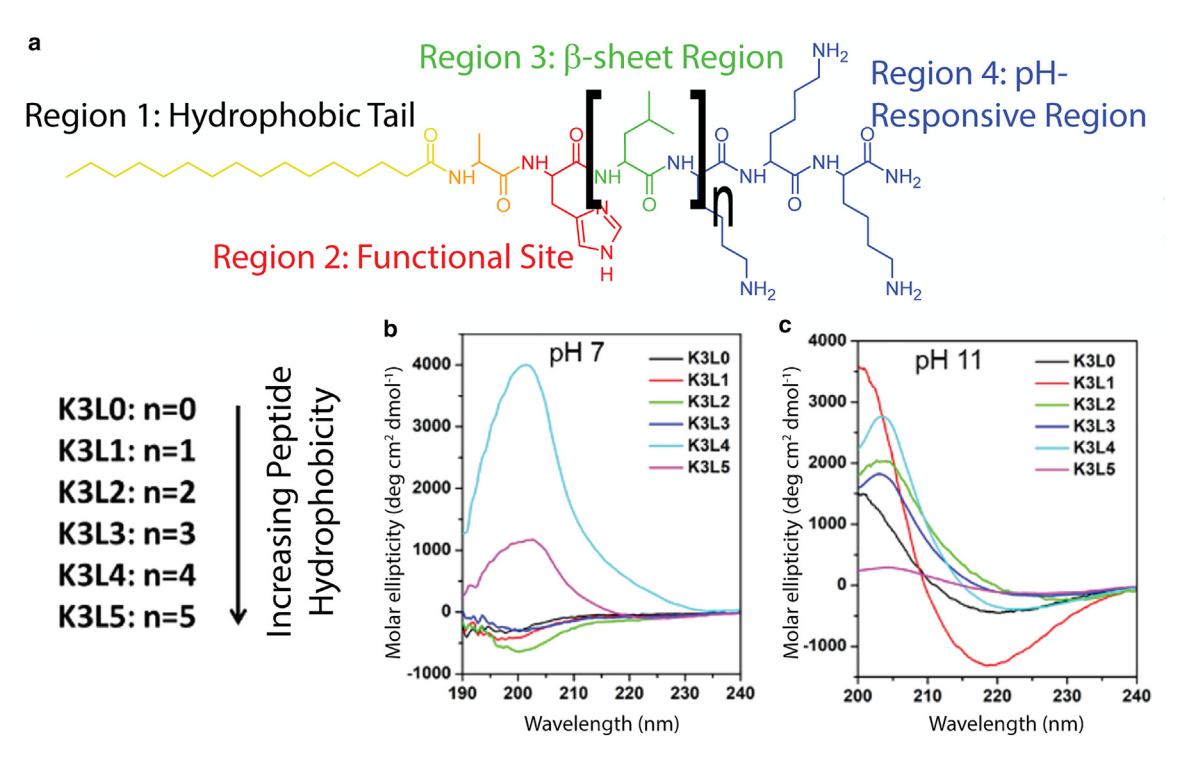


FIGURE 1 (a) Molecular structures of peptide amphiphiles with four rationally designed chemical moieties. Different components of the peptide amphiphile molecules are color coded as follows: palmitoyl (yellow), histidine (red), leucine (green), and lysine (blue). The heme-binding peptide amphiphiles were designed with variable Leu residues to study the effect of hydrophobic segment with heme binding and are named based on the number of Leu residues (n = 0, 1, 2, 3, 4, and 5). (b and c) The CD spectra of the peptide amphiphiles in free state were recorded at pH 7 and 11, revealing distinct conformational characteristics. At pH7, the spectra indicate an unstructured conformation, while at pH 11, a β-sheet conformation is observed, as indicated by characteristic peaks minima at 218 nm.

# Heme binding assay

Binding constants were determined by measuring the absorbance change of varying peptide concentrations in the presence of heme B. Peptide samples were prepared in either 10 mM HEPES buffer or 5 mM NH<sub>4</sub>OH, at pH 7 or 11, respectively. PA samples were diluted to varying concentrations of 0-1000  $\mu$ M, and heme B was added to each sample with a final concentration of 50  $\mu$ M. PA samples were then allowed to incubate at 90°C for 10 min and to cool to room temperature before being transferred to a clear 96-well plate. The absorbance was measured from 300 to 750 nm using a Tecan Spark microplate reader. The [peptide]/[heme] vs. absorption data were plotted, and the K<sub>D</sub> value was obtained using the loose-binding equation (Eq. 1) from the dose-response analysis package ("DRC") in R Studio (39).

$$[peptide : heme] = \frac{[PA] * [heme]}{K_D + [heme]}$$
 (Equation 1)

# Redox titration

The midpoint reduction potential (E<sub>M</sub>) of the peptide-heme complex was determined using spectroelectrochemistry (40,41). To achieve the peptide fibers, the peptide was dissolved in 5 mM NH<sub>4</sub>OH and incubated at 90°C for 10 min. 25  $\mu$ M heme was incorporated into the peptide solution at heme/PA molar ratios of 1:6 and 1:10, followed by further incubation at 90°C for 10 min. Mediators (phenazine methosulfate, gallocyanine, indigo carmine disulfate, 2-hydroxy-1,4-naphthoquinone, anthraquinone 2-sulfonate, benzyl viologen, methyl viologen, and anthraquinone) were added to the solution at a final concentration of 1 µM. Stock solutions of each mediator were prepared in DMSO. A small magnetic bar was added to the cuvette for constant stirring of the solution.

The heme-PA sample was placed in a 1 cm path length quartz cuvette. A platinum 3M Ag/AgCl combination electrode (Microelectrodes) was inserted through a septum in the cuvette for measuring the solution potential, and an N2 gas line was attached through the septum. The electrode was calibrated before insertion using saturated quinhydrone solutions at pH 7 and 4. The electrode potential was measured relative to the standard hydrogen electrode at 280 mV.

The absorbance was measured using ultraviolet-visible (UV-vis) spectroscopy. Sodium hydrosulfite (Na<sub>2</sub>S<sub>2</sub>O<sub>4</sub>) was used as a reducing agent, and a small aliquot of 1  $\mu$ L Na<sub>2</sub>S<sub>2</sub>O<sub>4</sub> was added to the solution per injection. The UV-vis absorbance spectrum and solution reduction/oxidation potential were measured after each injection. After complete reduction of the sample, potassium ferricyanide was added to oxidize the sample. The data were analyzed by taking the absorbance of the Q-band region (556 nm) and converting that into a Nernst curve depicting the fraction reduced. These titration curves were fitted to the Nernst equation to obtain the reduction midpoint potential. All titrations were repeated at least 24 h later with new peptide preparations to ensure reproducibility.

# **RESULTS**

# Peptide design and their characterization

To design our simplified heme-binding system, PAs were created based on previously reported self-assembling PAs: K3L3 (palmitic acid-AHLLLKKK) (36). The peptide sequence consists of four segments (Figs. 1 a and S2–S12; Table S1). The first is a hydrophobic tail—in this case,

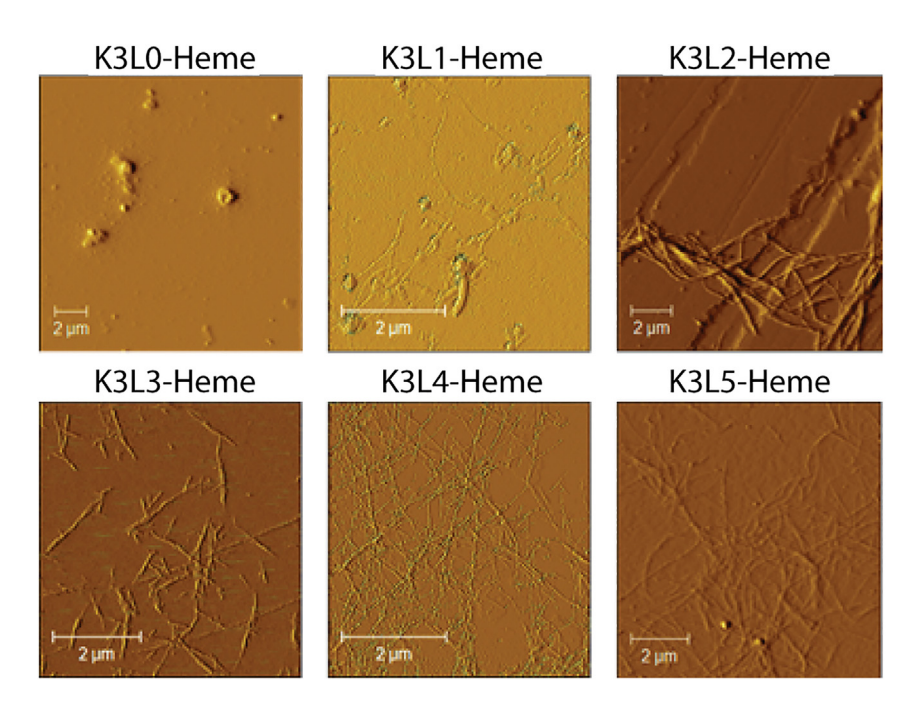


FIGURE 2 Characterization of peptide-heme complexes at pH 11. Peptides K3L1, K3L2, K3L3, K3L4, and K3L5 reveal fibrous structures. K3L0 exhibits an aggregated structure. Peptide-heme complexes were prepared in a 10:1 ratio in 5 mM NH<sub>4</sub>OH. AFM samples were then diluted to 10  $\mu M$  before being drop casted onto shaved mica surfaces. To see this figure in color, go online.

16-carbon palmitic acid—is attached to the N-terminus of the sequence to achieve hydrophobic collapse. The second is a hydrophobic structural region. Here, a β-sheet is formed that provides stability and is indicative of fiber formation (37,42). In this region, we kept the leucine residues, which have been shown to have the best cofactor binding properties, even though leucine residues are not commonly considered strong  $\beta$ -sheet-forming amino acids (43,44). The third section is environmentally responsive and is composed of three positively charged lysine residues. At pH 11, the Lys residues deprotonate, and the electrostatic repulsion between them is minimized, allowing  $\beta$ -sheets to form, which stabilizes the long polymeric fibrous structures (Figs. 2 and S13). The fourth section is the functional part of the peptide. A heme-binding site is introduced using the commonly employed histidine residue. Other ligation sets have been shown but have not been as thoroughly characterized (36,42). As we were primarily interested in the effects of sequence on the E<sub>M</sub>, we decided to maintain the alanine-histidine ligation set in this work, which also provides more established benchmarks to measure our results.

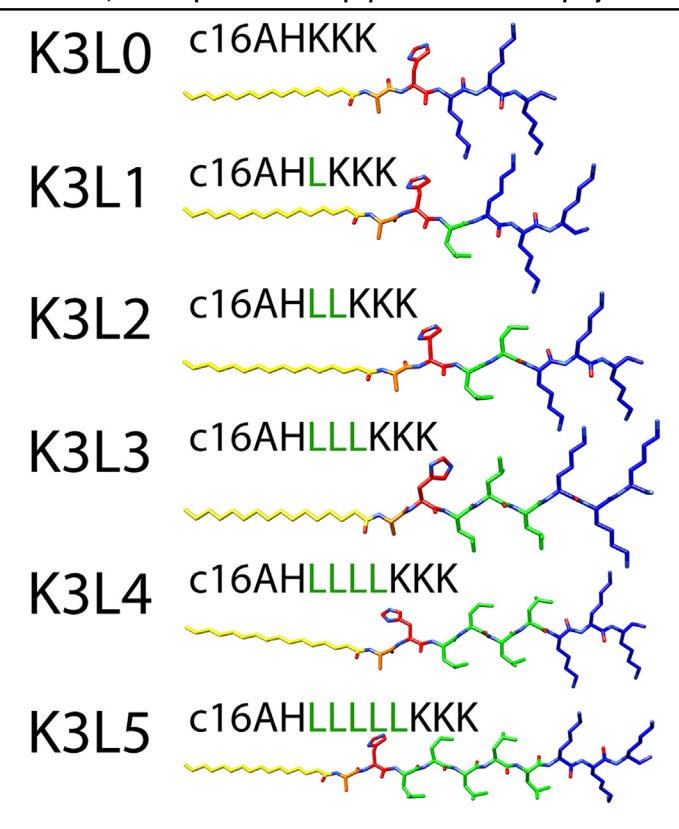
To better understand how the hydrophobic Leu region contributes to self-assembly and regulates the heme reduction potential, we designed and synthesized a series of K3L3 analogs (Table 1) with an increasing number of Leu. With these peptides, we aim to understand the effects of local hydrophobicity on peptide-heme assembly.

# Effect of leucine length on self-assembly

We explored the hydrophobic Leu region and its corresponding role in regulating the gross morphological structure. The supramolecular architectures of peptides are presumed to have a potential effect on modulating heme redox activity. Therefore, the self-assembled properties of six variants (K3L0-K3L5) were investigated at two different pHs, i.e., pH 7 and 11.

We employed CD to determine the secondary structures of PAs at pH 7 and 11 (Fig. 1, b and c). The characteristic peak at 218 nm indicates the presence of β-sheet structures, which has been shown to implicate fiber formation (35,42). Nevertheless, the CD spectra do not show a β-sheet conformation at pH 7 but rather an unstructured conformation (Fig. 1, b and c) for peptides K3L0-K3L3. However, for peptides K3L4 and K3L5, we note the presence of a β-sheet signal at pH 7, which we hypothesize is due to the one/two additional Leu residues. This provides a longer β-sheet region of the peptide, in turn providing more hydrogen bonds and additional hydrophobic character. The additional structural interactions overcome the electrostatic repulsion of the Lys residues. After an initial investigation into the secondary structure of peptides, we confirmed that the structure remained consistent when heme was bound to them (Fig. S13). In line with their free state, peptides K3L0– K3L3 displayed an unstructured conformation at pH 7, while K3L4 and K3L5 exhibited a β-sheet signal. However, at pH 11, all peptides showed an indication of fiber formation except for K3L0, which retained its unstructured conformation. AFM reveals that the variants K3L0-K3L3 exhibit a micelle-like structure at pH 7 and a fiber-like morphology at pH 11 (Fig. S14). Again, peptides K3L4 and K3L5 show a fiber-like morphology at pH 7 and fibrous structures at pH 11, supporting the CD data. At pH 11, the amine group in lysine is neutralized, eliminating the electrostatic repulsion and resulting in a transition from a micelle to fiber structure. We further analyzed the morphology of

TABLE 1 Abbreviated names, structures, and sequences of the peptides used in this project



peptide-heme complexes at pH 11, which yielded fibrous networks for peptide analogs K3L1–K3L5 (Fig. 2). In these peptides, we see larger structures of tangled peptides, which occurs due to the lack of electrostatic repulsion on the surface due to the neutralized Lys residues. However, K3L0 revealed a micelle-like structure, and this coincides with the weak  $\beta$ -sheet signal in CD. The lack of the hydrophobic region results in the difficulty with fiber formation. The utilization of a series of peptide variants allows for the examination of the influences of primary sequences on the self-assembly of peptides, the structure of peptide-heme complexes, and the functionality of heme binding.

# Binding constant analysis

To investigate the affinity of PAs to heme with length-dependent sequence variants and morphologies, we employed absorption spectroscopy to gain insight into heme insertion and ligand coordination. In both the fiber and micelle morphologies, all of the peptides exhibited a signature Soret peak (412 nm) and Q-band peaks (535 and 560 nm) (Figs. S15–S20). Peptides K3L1–K3L5 showed strong heme binding affinity in micellar structures at pH 7, indicating axial histidine ligation in the peptides (Table 2). The K3L0 micelles showed a weaker affinity, as indicated by the  $K_D$  value of 60  $\mu$ M at pH 7, which is

has a Z score of 2.12 compared to the rest of the data, indicating that it is significantly weaker. This observation can be attributed to the absence of the leucine region in K3L0, which resulted in lower hydrophobicity compared to the other PAs. The reduced hydrophobicity of K3L0 hindered the binding of heme at pH 7. However, at pH 11, the K3L0-heme binding  $K_D$  was comparable to the other five peptides.

Next, we explored the binding affinity of rigid fiber structures of PAs. In fibers, at pH 11, distinct Soret and Q-band peaks were observed, indicating the presence of 5-coordinate His coordination (Figs. S15–S20). We noticed that all peptide variants exhibit a similar binding affinity for heme at pH 11 (Table 2). Additionally, there was no significant trend for binding affinity in relation to the change in leucine-region length at either pH 7 or 11.

For all peptide variants that were tested, the data show the heme binding affinity to be in the low micromolar range. For future experiments, the heme concentration surpasses these values, ensuring our confidence that the heme remains bound throughout the duration of these experiments.

# Redox potentiometry

The  $E_M$  of heme was evaluated in the presence of PAs by spectroelectrochemical titrations (Fig. 3). We were

TABLE 2 The  $K_D$  values of heme B to the peptides used in this work

PAs	K <sub>D</sub> (μM)	
	pH 7	pH 11
K3L0	$60.0 \pm 0.7$	11.0 ± 1.3
K3L1	$4.2 \pm 0.3$	$13.0 \pm 0.3$
K3L2	$14 \pm 1$	$2.6 \pm 0.7$
K3L3	$22 \pm 2$	$9.0 \pm 2.7$
K3L4	$2.1 \pm 0.8$	$8.1 \pm 0.7$
K3L5	$11.0 \pm 1.8$	$5.5~\pm~0.7$

Binding titrations were carried out at both pH 7 and 11. Stronger binding is observed at pH 11 over pH 7.

interested in the potential impact of changes in heme environment and fiber stability on the heme  $E_M$ . Prior work has indicated a difference in ZnPPIX cofactor behavior is dependent upon their arrangement in the fiber matrix (42). We sought to investigate whether similar behavior is observed for heme B in various Leu environments. Notably, we observed a distinct change in the  $E_M$  at two distinct molar ratios: 1:6 and 1:10 heme/PA. These two molar ratios were selected based on previous work indicating that at a 1:6 loading ratio, ZnPPIX cofactors interact with one another, whereas that interaction is diminished at a loading ratio of 1:10. Due to significant light-scattering interference disrupting measurements, exceeding the 1:10 loading ratio was unfeasible.

UV-vis spectroscopy of oxidized heme shows a steady increase with  $\lambda_{max}$  at 429, 529, and 560 nm (Figs. 3 and S22–S27). All PA variants, K3L0, K3L1, K3L2, K3L3, K3L4, and K3L5, exhibit a higher E<sub>M</sub> value at a higher molar ratio of 1:10: -103, -78, -40, -69, -41, and -36 mV, respectively (Figs. 4 b and S22–S27). The variation in Leu length did not yield a significant effect on the  $E_{M}$  of the heme. Minimal fluctuations of  $E_{M}$  were observed with increasing hydrophobic segment in PAs, whereas a noticeable shift was evident with increased peptide concentration. This observation suggests that at a higher molar ratio (1:10), the metalloporphyrin site is well protected from the solvent and surrounded by a low-dielectric medium, which leads to the destabilization of the ferric state (45). Conversely, in highly polar and mobile aqueous environments, the ferric state is stabilized by solvent water molecules, resulting in a lower reduction potential at a lower molar ratio (1:6). The surface charge of the complex has also been shown to have an effect on the  $E_{M}$  (3). We suspect that not all of the Lys residues are fully deprotonated in the fibrous state, resulting in a positive charge on the fiber surface. This positive charge likely contributes to an increase in the E<sub>M</sub> value of heme in a similar fashion.

To ensure that the heme remained bound, we took reduced samples, spun them down, and looked at the spectra again. No spectra showed an appreciable loss of heme at either a 1:6 or 1:10 loading ratio (Table S2; Figs. S28 and

S29). Certain samples appeared to have slightly more reduced heme after spinning down, which we attribute to the removal of aggregated fibers that may have blocked light from getting through.

## CD analysis

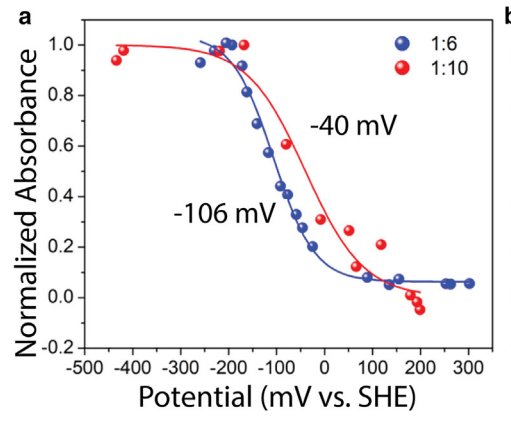
We were then interested in understanding how the stacking of hemes could lead to the observed increases in  $E_{\rm M}$ . To explore this, we employed CD spectroscopy, which reveals that when cofactors are stacked, they can form chiral structures that exhibit new properties distinct from their individual states

Past work has shown that adjusting the ratio of cofactor to peptide changes the cofactor stacking characteristics for ZnPPIX (46). At a ratio of 1:1 ZnPPIX/peptide, the cofactors are not wholly bound to the peptide and do not display any repetitive structure or CD signal. At intermediate ratios (i.e., 1:6 ZnPPIX/peptide), the cofactors are bound to the fiber and arranged in a chiral aggregate structure inside the peptide, which can be observed through CD. Finally, at higher ratios (1:10), the cofactors are dispersed throughout the fiber and do not stack on one another; thus, a noticeable CD signal is not observed. We confirmed these measurements with ZnPPIX in our K3L2 peptide here (Figs. 4 and S30).

Interestingly for peptides K3L1 and K3L2, the heme exhibits distinct behavior. At low concentrations of PAs (1:1 ratio), no CD signal is observed, aligning with our expectations from the ZnPPIX data. At a 1:6 ratio, which produced the highest CD signal for ZnPPIX, we observe a minimal signal with heme. However, upon increasing the heme loading to a 1:10 ratio, Cotton effect bands appear, indicating that the heme assumes a chiral orientation within the fiber bundle. This contrasts with ZnPPIX, which appears to form a chiral aggregate structure in the fiber matrix (Figs. 4 and S30) (46).

We hypothesize that in these peptides, at a 10:1 peptide/heme ratio, the heme becomes buried in a somewhat defined binding pocket within the fiber, assuming a specific chiral orientation. We further hypothesize that the propionate groups of heme are oriented toward the fiber surface due to the potential for charge pairing potential and lower hydrophobicity. The environment effectively stabilizes the reduced state. However, with an increased heme load, steric hinderance occurs as the hemes begin to disrupt one another, overcrowding the binding site. This leads to a loss of order withing the binding site, resulting in the diminished Cotton effect band. We suspect that this crowding allows more water into the system, thereby driving the reduction potential down, accounting for the drop we see in those values.

For peptides K3L3, K3L4, and K3L5, a more intense CD signal is observed at the 6:1 loading ratio (Fig. S30, c–e). This is likely due to the additional Leu residues stabilizing the binding site. Thus, even with additional heme crowding,



Peptide	Heme : Peptide	$E_{M}(mV)$
K3L0	1:6	-130 ± 3
	1:10 1:6	$\frac{-103 \pm 1}{-203 \pm 20}$
K3L1	1:10	-78 ± 6
K3L2	1:6 1:10	-106 ± 6 -40 ± 9
K3L3	1:10	-40 ± 9
	1:10	$-69 \pm 7$
K3L4	1:6	$-43 \pm 10$
K3L5	1:10 1:6	-41 ± 5 -146 ± 5
	1:10	$-36 \pm 4$

FIGURE 3 (a) Potentiometric titration of heme-K3L2 complexes was performed at pH 11. Heme was fixed at 15  $\mu$ M, and peptide was added at molar ratios of 1:6 (90  $\mu$ M) and 1:10 (150  $\mu$ M), respectively. All experiments were carried out at 22°C in 125 mM NH<sub>4</sub>OH buffer (pH 11) or 10 mM HEPES buffer (pH 7). The results demonstrated that the presence of heme B had a significant effect on the incorporation of peptide K3L2, leading to changes in the reduction potential. Notably, the reduction potential of heme B exhibited significant variations with the change in heme-K3L2 molar ratios, indicating the influence of peptide structures in coordinating with heme B. (b) The list provides the midpoint potentials (E<sub>M</sub>) of heme B in the presence of different peptides. A diverse range of midpoint

potentials was observed, depending on the peptide sequences and morphologies. Notably, a higher midpoint potential was observed at a higher heme/peptide molar ratio of 1:10, indicating that heme B was buried and less accessible to the solvent.

the fiber can maintain a stable binding pocket, retaining the chiral orientation of heme.

### DISCUSSION

We have generated a model peptide system in which we can tailor the reduction/oxidation properties of bound heme cofactors. To understand the influence of the  $\beta$ -sheet region, we have synthesized a number of peptide variants containing different hydrophobic segments. Changing the peptide sequence by simply changing how much heme is added into the fiber showed significant changes to the reduction midpoint potential. We showed ranges of up to 100 mV difference when we increased the molar ratio from 1:6 to 1:10. The rise in the midpoint potential indicates that the metalloporphyrin is buried and protected from external solvents. However, for peptides K3L2-K3L5, no significant changes (i.e., no Z score greater than or equal to 2) were observed when employing different lengths of the hydrophobic β-sheet segment. This suggests that the peptide assemblies in this paper create a similar hydrophobic pocket regardless of the length of the Leu region. We observed that K3L0 has slightly lower potentials (-103 mV). Though still relatively high, these are lower than K3L2 (-40 mV). We attribute this difference to the lack of a hydrophobic pocket and the accessibility of water in the heme site.

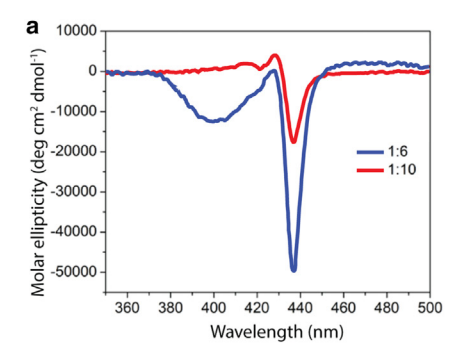
The differences we see when going from 1:6 to 1:10 go as high as 124 mV. In the context of natural proteins, this difference is significant. Bonaventura et al. discuss the effect of changing the  $E_{\rm M}$  on oxygen binding and side reactions that are caused by a change in the heme midpoint potential (47). In that work, they show that hemoglobin A in two different conditions has an  $E_{\rm M}$  split of approximately 40 mV, which leads to a 10-fold difference in affinity for oxygen. Our peptides have a range of differences that indicate there would be clear functional changes in similar circumstances.

The  $E_M$  of heme in these fiber systems is controlled by a variety of factors. The most impactful parameter is heme

loading, which affects almost all of the fiber sequences, showing E<sub>M</sub> differences up to 125 mV for the K3L1 peptide. Past work has shown that moving heme cofactors into close proximity or stacking aromatic molecules on heme increase the potential (3,48); however, in our system, we see the opposite effect. This can most readily be explained by the stacking hemes creating a small yet bulky porphyrin structure that mildly disrupts the binding site and allows water to access the heme itself, thereby driving down the potential (1). We did not observe any changes in the morphology, so we do not believe that the  $\beta$ -sheet interactions nor the fiber's shape are impacted by this. The spectra of heme we have in our fibers do not match the Jor H-aggregate spectra of heme B seen elsewhere (49,50). We attribute this to the lack of His ligation in those aggregates, whereas in our fiber, the hypothesized heme structure appears to have His ligands based on similarities to established heme B UV-vis spectra (Figs. S15–S20) (3,36). Similarly, our fibers do not show similar spectra to the OmcS protein itself (51), which we attribute to the lack of bis-His ligands in our fibers (36).

The peptides K3L0, K3L1, K3L2, K3L3, and K3L5 all have  $E_M$  splits ranging from 26.5 to 124 mV. However, **K3L4** has a noticeably low difference of 2.5 mV. We attribute this to the structure of the peptide inhibiting formation of any porphyrin structure. As noted in the CD spectra (Fig. S30), K3L4 does not display any Cotton effect signal in either heme/peptide ratio. Further studies are needed to determine why the **K3L4** peptide is inhibiting this structure and how that affects the electrochemical properties of heme B.

Previous work measured the  $E_M$  of the K3L3 peptide at a 6:1 peptide/heme loading ratio to be -655 mV, far lower than the data we show here (36). We believe that this discrepancy stems from the spectral-electrochemical cell not having space for a stir bar in the previous experiments. In this case, the fibers, which are prone to aggregation, may have crashed out of the solution. The resulting low measured



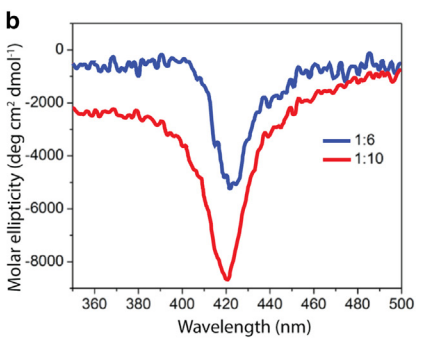


FIGURE 4 CD spectra of **K3L2** with ZnPPIX (a) and heme (b) monitored by CD spectroscopy. CD spectra of 50 µM ZnPPIX or 50 µM heme in 15 mM NH<sub>4</sub>OH with 300 and 500  $\mu$ M K3L2. Spectra were taken at room temperature.

potential could thus be the result of slow reduction kinetics leading to a mismatch in the environmental E<sub>H</sub> and the oxidation state of the heme cofactor. In the current work, all titrations were run with a stir bar, which kept the fibers from aggregating and falling out of the solution.

Currently there are many groups looking into long-range electron transport proteins such as MtrCAB and OmcS (20,38,51). Our system can serve as a simplified model system for these processes where the properties of the cofactors (e.g., heme stacking, E<sub>M</sub>) can be tuned and electron transport can be modeled to understand how these parameters are linked. It is important in these systems to tune the potential, as it may influence the ability for these fibers to accept or donate electrons from certain electrodes or other environmental contaminants.

For example, many studies have been done trying to understand why heme is spaced out as it is in the OmcS protein and the implications for long-range electron transport and, by extension, bioremediation functions (21,31,52,53). Here, we show that a significant overlap of heme cofactors can dramatically lower the E<sub>M</sub>. The coupling of heme cofactors in the OmcS protein is responsible for its low potential of  $-200 \,\mathrm{mV}$  (54). In our system, we show that spacing those cofactors out and burying them in a hydrophobic core under a positively charged surface leads to much higher potentials that could impede long-range electron transport in these systems, confirming those other results. The protein structure therefore may be tuned to promote some overlap in this way to tune the potential.

The implications from our new understanding of this material are immense. Several heme-based reactions are constantly being exploited for industrial purposes including waste processing, drug production, chemical synthesis of flavors and fragrances, polymer synthesis, bioremediation, and more (55-62). It has also been used for medical purposes including artificial oxygen carriers and diagnostics (63-67). With such control over the redox properties, we are setting up PAs to meet many of these needs through simple modifications. These principles could be used to develop artificial oxygen carriers (16,68), as the ability to reversibly bind molecular oxygen, and not form reactive oxygen species, is tightly linked to the  $E_M$  (47,63).

Similarly, the modifications that would allow the fibers we have produced to transport electrons could be used in a variety of areas, most directly in the generation of new bioelectronic technologies where peptides can be used in place of wires for microbial fuel cells (40,41,69,70). OmcS proteins have been implicated in the transfer of electrons from the bacteria to the electrode in these systems (71), and we hypothesize that the tunability of our fibers and the range of potentials can create microbial fuel cells with different voltage and current outputs.

As mentioned above, OmcS and MtrCAB play a role in the bioremediation of water. Similarly, the fibers we present here could also play a role in the bioremediation of water by transporting electrons to metal ions and removing impurities. Our new understanding and insights have led to us being able to tune the pH stability of our fibers and the E<sub>M</sub> values of bound redox cofactors. Other groups can use these findings to create materials or polymeric systems where specific analytes can be reacted with based on their  $E_{M}$  values.

In conclusion, we designed and synthesized PAs that selfassemble and bind the redox-active cofactor heme B. Using different sequences and heme/peptide molar ratios, we regulated the heme's reduction and oxidation properties. The midpoint potential of heme-bound PAs suggests a similar heme environment. We believe that this system can both serve as a model system for natural proteins and lead to new biomaterials and biotechnologies that incorporate high-potential heme cofactors.

# **CONCLUSIONS**

We have successfully characterized a PA material, establishing it as a model system for studying long-range electron transport phenomena in natural proteins. This material holds significant promise for advancing such studies, offering an accessible tool for making small but impactful modifications and examining their effects without concern about protein misfolding or other artifacts. Similarly, this material holds potential for further development, particularly incorporating new functions using the versatile redox cofactor heme B. This could lead to the creation of functional materials with applications ranging from waste purification to biomedical functions.

# **SUPPORTING MATERIAL**

Supporting material can be found online at https://doi.org/10.1016/j.bpj. 2024 05 021

### **FUNDING**

This work was supported by NSF CAREER award BMAT 2041751 (all peptide synthesis and redox titrations), and CHRB award 247-01-21 (AFM and CD).

### **AUTHOR CONTRIBUTIONS**

Development of project and conceptualization, C.D., V.L., and L.A.S.; preparation of peptides, C.D., V.L., A.M.R., C.P., A.C., and N.R.; purification of peptides, C.D., V.L., A.M.R., C.P., A.C., and N.R.; CD analysis, C.D., V.L., A.M.R., and N.R.; AFM, C.D., V.L., and A.M.R.; heme binding titrations, V.L. and A.M.R.; redox potentiometry, C.D., V.L., A.M.R., and C.P.; preparation of manuscript, V.L., C.D., and L.A.S.

### **ACKNOWLEDGMENTS**

The authors would like to thank Dr. Joel Schnur for his insights and help editing the manuscript.

# **DECLARATION OF INTERESTS**

The authors declare no competing interests.

### **REFERENCES**

- Shifman, J. M., B. R. Gibney, ..., P. L. Dutton. 2000. Heme Redox Potential Control in de Novo Designed Four-α-Helix Bundle Proteins. *Biochemistry*. 39:14813–14821. https://doi.org/10.1021/bi000927b.
- Lu, Y., N. Yeung, ..., N. M. Marshall. 2009. Design of Functional Metalloproteins. *Nature*. 460:855–862. https://doi.org/10.1038/nature08304.
- Solomon, L. A., J. Witten, ..., P. L. Dutton. 2022. Tailorable Tetrahelical Bundles as a Toolkit for Redox Studies. *J. Phys. Chem. B*. 126:8177–8187. https://doi.org/10.1021/acs.jpcb.2c05119.
- Bhagi-Damodaran, A., J. H. Reed, ..., Y. Lu. 2018. Heme Redox Potentials Hold the Key to Reactivity Differences between Nitric Oxide Reductase and Heme-Copper Oxidase. *Proc. Natl. Acad. Sci. USA*. 115:6195–6200. https://doi.org/10.1073/pnas.1720298115.
- Hutchins, G. H., C. E. M. Noble, M. P. Crump..., 2020. Precision design of single and multi-heme de novo proteins. Preprint at Synthetic Biol. https://doi.org/10.1101/2020.09.24.311514.
- Solomon, L. A., G. Kodali, ..., P. L. Dutton. 2014. Engineering the Assembly of Heme Cofactors in Man-Made Proteins. *J. Am. Chem. Soc.* 136:3192–3199. https://doi.org/10.1021/ja411845f.
- Bhagi-Damodaran, A., I. D. Petrik, ..., Y. Lu. 2014. Systematic Tuning of Heme Redox Potentials and Its Effects on O2 Reduction Rates in a Designed Oxidase in Myoglobin. J. Am. Chem. Soc. 136:11882–11885. https://doi.org/10.1021/ja5054863.
- 8. Reedy, C. J., and B. R. Gibney. 2004. Heme Protein Assemblies. *Chem. Rev.* 104:617–649. https://doi.org/10.1021/cr0206115.

- Huang, X., and J. T. Groves. 2018. Oxygen Activation and Radical Transformations in Heme Proteins and Metalloporphyrins. *Chem. Rev.* 118:2491–2553. https://doi.org/10.1021/acs.chemrev.7b00373.
- Shimizu, T., A. Lengalova, ..., M. Martínková. 2019. Heme: emergent roles of heme in signal transduction, functional regulation and as catalytic centres. *Chem. Soc. Rev.* 48:5624–5657. https://doi.org/10.1039/ C9CS00268E.
- Gibney, B. R., F. Rabanal, ..., P. L. Dutton. 1998. Effect of Four Helix Bundle Topology on Heme Binding and Redox Properties. *Biochemistry*. 37:4635–4643. https://doi.org/10.1021/bi971856s.
- Korendovych, I. V., and W. F. DeGrado. 2020. De Novo Protein Design, a Retrospective. Q. Rev. Biophys. 53:e3. https://doi.org/10.1017/ S0033583519000131.
- 13. Chino, M., S.-Q. Zhang, ..., W. F. DeGrado. 2018. Spectroscopic and Metal Binding Properties of a de Novo Metalloprotein Binding a Tetrazinc Cluster. *Biopolymers*. 109: e23339. https://doi.org/10.1002/bip.23229.
- Farid, T. A., G. Kodali, ..., P. L. Dutton. 2013. Elementary Tetrahelical Protein Design for Diverse Oxidoreductase Functions. *Nat. Chem. Biol.* 9:826–833. https://doi.org/10.1038/nchembio.1362.
- Anderson, J. L. R., C. T. Armstrong, ..., P. L. Dutton. 2014. Constructing a Man-Made c-Type Cytochrome Maquette in Vivo: Electron Transfer, Oxygen Transport and Conversion to a Photoactive Light Harvesting Maquette. *Chem. Sci.* 5:507–514. https://doi.org/10.1039/C3SC52019F.
- Koder, R. L., J. L. R. Anderson, ..., P. L. Dutton. 2009. Design and Engineering of an O2 Transport Protein. *Nature*. 458:305–309. https://doi.org/10.1038/nature07841.
- Chen, Y. X., N. L. Ing, ..., D. J. Glover. 2020. Structural Determination of a Filamentous Chaperone to Fabricate Electronically Conductive Metalloprotein Nanowires. ACS Nano. 14:6559–6569. https://doi.org/ 10.1021/acsnano.9b09405.
- Malvankar, N. S., M. Vargas, ..., D. R. Lovley. 2011. Tunable Metallic-like Conductivity in Microbial Nanowire Networks. *Nat. Nanotechnol.* 6:573–579. https://doi.org/10.1038/nnano.2011.119.
- Edwards, M. J., G. F. White, ..., T. A. Clarke. 2020. The Crystal Structure of a Biological Insulated Transmembrane Molecular Wire. *Cell*. 181:665–673.e10. https://doi.org/10.1016/j.cell.2020.03.032.
- Jiang, X., J. H. van Wonderen, ..., J. Blumberger. 2020. Which Multi-Heme Protein Complex Transfers Electrons More Efficiently? Comparing MtrCAB from Shewanella with OmcS from Geobacter. J. Phys. Chem. Lett. 11:9421–9425. https://doi.org/10.1021/acs.jpclett.0c02842.
- Dahl, P. J., S. M. Yi, ..., N. S. Malvankar. 2022. A 300-Fold Conductivity Increase in Microbial Cytochrome Nanowires Due to Temperature-Induced Restructuring of Hydrogen Bonding Networks. Sci. Adv. 8, eabm7193. https://doi.org/10.1126/sciadv.abm7193.
- Baker, D. 2019. What Has de Novo Protein Design Taught Us about Protein Folding and Biophysics? *Protein Sci.* 28:678–683. https://doi. org/10.1002/pro.3588.
- Lichtenstein, B. R., T. A. Farid, ..., P. L. Dutton. 2012. Engineering Oxidoreductases: Maquette Proteins Designed from Scratch. *Biochem.* Soc. Trans. 40:561–566. https://doi.org/10.1042/BST20120067.
- Coluzza, I. 2017. Computational Protein Design: A Review. J. Phys. Condens. Matter. 29: 143001. https://doi.org/10.1088/1361-648X/aa5c76.
- Ferrando, J., and L. A. Solomon. 2021. Recent Progress Using De Novo Design to Study Protein Structure, Design and Binding Interactions. *Life*. 11:225. https://doi.org/10.3390/life11030225.
- Lucas, J. E., and T. Kortemme. 2020. New Computational Protein Design Methods for de Novo Small Molecule Binding Sites. *PLoS Comput. Biol.* 16: e1008178. https://doi.org/10.1371/journal.pcbi. 1008178.
- Mirts, E. N., A. Bhagi-Damodaran, and Y. Lu. 2019. Understanding and Modulating Metalloenzymes with Unnatural Amino Acids, Non-Native Metal Ions, and Non-Native Metallocofactors. Acc. Chem. Res. 52:935–944. https://doi.org/10.1021/acs.accounts.9b00011.

- Grayson, K. J., and J. L. R. Anderson. 2018. Designed for Life: Biocompatible de Novo Designed Proteins and Components. J. R. Soc. Interface. 15: 20180472. https://doi.org/10.1098/rsif.2018.0472.
- Grayson, K. J., and J. R. Anderson. 2018. The Ascent of Man(Made Oxidoreductases). Curr. Opin. Struct. Biol. 51:149–155. https://doi. org/10.1016/j.sbi.2018.04.008.
- Sakurai, T., S. Sakaguchi, ..., S. Seki. 2020. Porphyrin Nanowire Bundles for Efficient Photoconductivity, Photoemission, and Generation of Singlet Oxygens toward Photodynamic Therapy. ACS Appl. Nano Mater. 3:6043–6053. https://doi.org/10.1021/acsanm.0c01242.
- Chen, Z., J.-R. Deng, ..., J. O. Thomas. 2023. Phase-Coherent Charge Transport through a Porphyrin Nanoribbon. J. Am. Chem. Soc. 145:15265–15274. https://doi.org/10.1021/jacs.3c02451.
- Breuer, M., K. M. Rosso, and J. Blumberger. 2014. Electron Flow in Multiheme Bacterial Cytochromes Is a Balancing Act between Heme Electronic Interaction and Redox Potentials. *Proc. Natl. Acad. Sci.* USA. 111:611–616. https://doi.org/10.1073/pnas.1316156111.
- Guberman-Pfeffer, M. J. 2022. Assessing Thermal Response of Redox Conduction for *Anti* -Arrhenius Kinetics in a Microbial Cytochrome Nanowire. *J. Phys. Chem. B.* 126:10083–10097. https://doi.org/10. 1021/acs.jpcb.2c06822.
- Cui, H., M. J. Webber, and S. I. Stupp. 2010. Self-Assembly of Peptide Amphiphiles: From Molecules to Nanostructures to Biomaterials. *Bio-polymers*. 94:1–18. https://doi.org/10.1002/bip.21328.
- Hendricks, M. P., K. Sato, ..., S. I. Stupp. 2017. Supramolecular Assembly of Peptide Amphiphiles. Acc. Chem. Res. 50:2440–2448. https://doi.org/10.1021/acs.accounts.7b00297.
- Solomon, L. A., J. B. Kronenberg, and H. C. Fry. 2017. Control of Heme Coordination and Catalytic Activity by Conformational Changes in Peptide-Amphiphile Assemblies. *J. Am. Chem. Soc.* 139:8497–8507. https://doi.org/10.1021/jacs.7b01588.
- Solomon, L. A., A. R. Wood, ..., H. C. Fry. 2019. Microenvironment Control of Porphyrin Binding, Organization, and Function in Peptide Nanofiber Assemblies. *Nanoscale*. 11:5412–5421. https://doi.org/10. 1039/C8NR09556F.
- Wang, F., Y. Gu, ..., N. S. Malvankar. 2019. Structure of Microbial Nanowires Reveals Stacked Hemes That Transport Electrons over Micrometers. Cell. 177:361–369.e10. https://doi.org/10.1016/j.cell.2019. 03.029.
- Sørensen, H., N. Cedergreen, ..., J. C. Streibig. 2007. An Isobole-Based Statistical Model and Test for Synergism/Antagonism in Binary Mixture Toxicity Experiments. *Environ. Ecol. Stat.* 14:383–397. https://doi.org/10.1007/s10651-007-0022-3.
- Richter, H., K. P. Nevin, ..., L. M. Tender. 2009. Cyclic Voltammetry of Biofilms of Wild Type and Mutant Geobacter Sulfurreducens on Fuel Cell Anodes Indicates Possible Roles of OmcB, OmcZ, Type IV Pili, and Protons in Extracellular Electron Transfer. *Energy Environ. Sci.* 2:506. https://doi.org/10.1039/b816647a.
- Tatinclaux, M., K. Gregoire, ..., B. V. Kjellerup. 2018. Electricity Generation from Wastewater Using a Floating Air Cathode Microbial Fuel Cell. Water-Energy Nexus. 1:97–103. https://doi.org/10.1016/j.wen. 2018.09.001.
- Fry, H. C., J. M. Garcia, ..., S. I. Stupp. 2012. Self-Assembly of Highly Ordered Peptide Amphiphile Metalloporphyrin Arrays. *J. Am. Chem.* Soc. 134:14646–14649. https://doi.org/10.1021/ja304674d.
- D'Souza, A., X. Wu, ..., S. Bhattacharjya. 2017. Designed Heme-Cage β-Sheet Miniproteins. Angew. Chem. Int. Ed. 56:5904–5908. https:// doi.org/10.1002/anie.201702472.
- D'Souza, A., J. Torres, and S. Bhattacharjya. 2018. Expanding Heme-Protein Folding Space Using Designed Multi-Heme β-Sheet Mini-Proteins. *Commun. Chem.* 1:78. https://doi.org/10.1038/s42004-018-0078-z.
- Ghirlanda, G., A. Osyczka, ..., W. F. DeGrado. 2004. De Novo Design of a D2-Symmetrical Protein That Reproduces the Diheme Four-Helix Bundle in Cytochrome Bc1. J. Am. Chem. Soc. 126:8141–8147. https:// doi.org/10.1021/ja039935g.

- Fry, H. C., J. M. Garcia, ..., S. I. Stupp. 2012. Self-Assembly of Highly Ordered Peptide Amphiphile Metalloporphyrin Arrays. J. Am. Chem. Soc. 134:14646–14649. https://doi.org/10.1021/ja304674d.
- Bonaventura, C., R. Henkens, ..., A. L. Crumbliss. 2013. Molecular Controls of the Oxygenation and Redox Reactions of Hemoglobin. *Antioxidants Redox Signal*. 18:2298–2313. https://doi.org/10.1089/ars. 2012.4947.
- Weinert, E. E., C. M. Phillips-Piro, and M. A. Marletta. 2013. Porphyrin π-Stacking in a Heme Protein Scaffold Tunes Gas Ligand Affinity. J. Inorg. Biochem. 127:7–12. https://doi.org/10.1016/j.jinorg-bio.2013.06.004.
- 49. Teixeira, R., S. M. Andrade, ..., S. M. B. Costa. 2012. Reorganization of Self-Assembled Dipeptide Porphyrin J-Aggregates in Water–Ethanol Mixtures. *J. Phys. Chem. B.* 116:2396–2404. https://doi.org/10.1021/jp2115719.
- Mabesoone, M. F. J., A. J. Markvoort, ..., E. W. Meijer. 2018. Competing Interactions in Hierarchical Porphyrin Self-Assembly Introduce Robustness in Pathway Complexity. J. Am. Chem. Soc. 140:7810–7819. https://doi.org/10.1021/jacs.8b02388.
- Qian, X., T. Mester, ..., D. R. Lovley. 2011. Biochemical Characterization of Purified OmcS, a c-Type Cytochrome Required for Insoluble Fe(III) Reduction in Geobacter Sulfurreducens. *Biochim. Biophys. Acta.* 1807:404–412. https://doi.org/10.1016/j.bbabio.2011.01.003.
- Sedghi, G., V. M. García-Suárez, ..., R. J. Nichols. 2011. Long-Range Electron Tunnelling in Oligo-Porphyrin Molecular Wires. *Nat. Nano-technol.* 6:517–523. https://doi.org/10.1038/nnano.2011.111.
- Neu, J., C. C. Shipps, ..., N. S. Malvankar. 2022. Microbial Biofilms as Living Photoconductors Due to Ultrafast Electron Transfer in Cytochrome OmcS Nanowires. *Nat. Commun.* 13:5150. https://doi.org/10. 1038/s41467-022-32659-5.
- Guberman-Pfeffer, M. J. 2023. Structural Determinants of Redox Conduction Favor Robustness over Tunability in Microbial Cytochrome Nanowires. *J. Phys. Chem. B.* 127:7148–7161. https://doi.org/10.1021/acs.jpcb.3c02912.
- Schmitz, L. M., K. Rosenthal, and S. Lütz. 2019. Recent Advances in Heme Biocatalysis Engineering. *Biotechnol. Bioeng*. 116:3469–3475. https://doi.org/10.1002/bit.27156.
- Bajaj, P., G. Sreenilayam, ..., R. Fasan. 2016. Gram-Scale Synthesis of Chiral Cyclopropane-Containing Drugs and Drug Precursors with Engineered Myoglobin Catalysts Featuring Complementary Stereoselectivity. Angew. Chem. Int. Ed. 55:16110–16114. https://doi.org/10. 1002/anie.201608680.
- Schröder, G. C., M. S. Smit, and D. J. Opperman. 2023. Harnessing Heme Chemistry: Recent Advances in the Biocatalytic Applications of Cytochrome P450 Monooxgenases. *Curr. Opin. Green Sustainable Chem.* 39: 100734. https://doi.org/10.1016/j.cogsc.2022.100734.
- Gomez De Santos, P., M. Cañellas, ..., M. Alcalde. 2018. Selective Synthesis of the Human Drug Metabolite 5'-Hydroxypropranolol by an Evolved Self-Sufficient Peroxygenase. ACS Catal. 8:4789–4799. https://doi.org/10.1021/acscatal.8b01004.
- Gomez De Santos, P., F. V. Cervantes, ..., M. Alcalde. 2019. Benchmarking of Laboratory Evolved Unspecific Peroxygenases for the Synthesis of Human Drug Metabolites. *Tetrahedron*. 75:1827–1831. https://doi.org/10.1016/j.tet.2019.02.013.
- Wang, S., L. Qiu, ..., R. Qiu. 2018. Electron Transport Chains in Organohalide-Respiring Bacteria and Bioremediation Implications. *Biotechnol. Adv.* 36:1194–1206. https://doi.org/10.1016/j.biotechadv. 2018.03.018.
- 61. Yun, J., N. S. Malvankar, ..., D. R. Lovley. 2016. Functional Environmental Proteomics: Elucidating the Role of a c-Type Cytochrome Abundant during Uranium Bioremediation. *ISME J.* 10:310–320. https://doi.org/10.1038/ismej.2015.113.
- Lin, Y.-W. 2020. Rational Design of Heme Enzymes for Biodegradation of Pollutants toward a Green Future. *Biotechnol. Appl. Biochem.* 67:484

  –494. https://doi.org/10.1002/bab.1788.
- Dorman, S. C., C. F. Kenny, ..., J. P. Harrington. 2002. Role of Redox Potential of Hemoglobin-Based Oxygen Carriers on Methemoglobin

- Reduction by Plasma Components. *Artif. Cells Blood Substit. Immobil. Biotechno.* 30:39–51. https://doi.org/10.1081/bio-120002726.
- Zhang, L., J. L. R. Anderson, ..., R. L. Koder. 2011. Manipulating Cofactor Binding Thermodynamics in an Artificial Oxygen Transport Protein. *Biochemistry*. 50:10254–10261. https://doi.org/10.1021/ bi201242a.
- Immenschuh, S., V. Vijayan, ..., F. Gueler. 2017. Heme as a Target for Therapeutic Interventions. *Front. Pharmacol.* 8:146. https://doi.org/10. 3389/fphar.2017.00146.
- Heckl, C., M. Eisel, ..., R. Sroka. 2021. Spectroscopic Methods to Quantify Molecules of the Heme-biosynthesis Pathway: A Review of Laboratory Work and Point-of-care Approaches. *Transl. Biophotonics*. 3: e202000026. https://doi.org/10.1002/tbio.202000026.
- 67. Munoz, C., F. Aletti, ..., E. B. Kistler. 2020. Resuscitation After Hemorrhagic Shock in the Microcirculation: Targeting Optimal Oxygen De-

- livery in the Design of Artificial Blood Substitutes. *Front. Med.* 7: 585638. https://doi.org/10.3389/fmed.2020.585638.
- 68. Alayash, A. I. 1999. Review. 1999:545-549.
- Boas, J. V., V. B. Oliveira, ..., A. M. F. R. Pinto. 2022. Review on Microbial Fuel Cells Applications, Developments and Costs. *J. Environ. Manag.* 307: 114525. https://doi.org/10.1016/j.jenvman.2022.114525.
- Bazina, N., T. G. Ahmed, ..., M. Sarker. 2023. Power Generation from Wastewater Using Microbial Fuel Cells: A Review. *J. Biotechnol.* 374:17–30. https://doi.org/10.1016/j.jbiotec.2023.07.006.
- Krige, A., M. Sjöblom, ..., U. Rova. 2019. On-Line Raman Spectroscopic Study of Cytochromes' Redox State of Biofilms in Microbial Fuel Cells. *Molecules*. 24:646. https://doi.org/10.3390/molecules24030646.